57th EASTERN SNOW CONFERENCE
Syracuse, New York, USA, 2000

Winter Season Variability in North American Prairie SWE Distribution and Atmospheric Circulation

C. DERKSEN,[1] E. LEDREW,[1] A. WALKER,[2] AND B. GOODISON[2]

ABSTRACT

Ten winter seasons (December, January, February 1988/89 to 1997/98) of five-day averaged (pentad) passive-microwave derived SWE imagery are utilized to examine the seasonal snow cover characteristics of a ground-validated North American Prairie study area. Principal components analysis (PCA) is used to identify the dominant spatial patterns through time for three passive-microwave derived datasets: (1) pentad SWE, (2) pentad SWE anomalies based on the 10 season mean and standard deviation, and (3) change-in-pentad SWE (ΔSWE) calculated by subtracting each SWE pattern from the previous. Interpretation of the component loading patterns indicates that the ΔSWE time series is best suited for the climatological application of identifying associations between snow cover and atmospheric circulation. Two dominant patterns are identified within the ΔSWE time series: the positive (negative) phase of principal component 1 captures a pattern of widespread SWE ablation (accumulation) in the south with accumulation (ablation) to the north. The positive (negative) phase of principal component two characterizes a meridional accumulation (ablation) zone oriented from the northwest to southeast of the study area. An investigation of composite and anomaly atmospheric fields illustrates that unique and consistent atmospheric circulation patterns are linked to the ΔSWE components.

Key Words: Atmospheric circulation, Passive-microwave, Snow water equivalent

[1] Waterloo Laboratory for Earth Observations, Department of Geography, University of Waterloo, Waterloo, Ontario N2L 3G1, CANADA
email: chris@watleo.uwaterloo.ca

[2] Climate Research Branch, Meteorological Service of Canada, 4905 Dufferin Street, Downsview, Ontario M3H 5T4, Ontario, CANADA

INTRODUCTION

With a high degree of seasonal and interannual variability in spatial extent, identifying associations between elements of the cryosphere and the atmosphere is essential for understanding, modelling, and predicting the global climate system. The investigation of terrestrial snow cover is particularly intriguing because of the complex nature of the interaction between snow on the earth's surface and atmospheric circulation. While the presence or absence of snow cover modifies energy exchange with overlying air masses, it is these air masses themselves which deposit and ablate snow cover. With unique physical processes such as a high surface albedo (in open areas) and low thermal conductivity, general circulation models must accurately portray the extent, magnitude, and variability of terrestrial snow cover to realistically capture the role of snow cover in large-scale climate processes.

In addition to the climatological role, significant hydrological processes are also influenced by snow cover, which acts as the frozen storage term in the water balance. Water is thereby held for a potentially lengthy period before it actively enters a hydrological system through runoff. Productive agricultural regions such as the Canadian Prairies rely heavily on spring meltwater for crop irrigation. Unlike rainfall, solid precipitation is modified by additional snow accumulation, wind redistribution, and other meteorological events before entering the liquid phase. The synergy between global energy and water cycles, and the important role that terrestrial snow cover plays in both of these cycles, enforces the need for spatially continuous, temporally repetitive, and synoptically sensitive observation of snow cover to adequately monitor these systems. To meet these data objectives, remote sensing has been utilized as a data source for examining variability and change in both the cryosphere as a whole, and terrestrial snow cover specifically.

The characteristics of passive-microwave remote sensing provide a number of advantages over snow cover datasets based on optical remote sensing. All-weather imaging, rapid scene revisit, and the ability to derive quantitative estimates of snow water equivalent (SWE) has motivated a significant research effort in passive-microwave algorithm development for the retrieval of snow cover parameters (for example, Chang et al., 1990; Goodison and Walker, 1994; Grody and Basist, 1996; Tait, 1998). The ability to map SWE is particularly significant because of the importance of snow depth over snow extent for hydrological, climatological, and meteorological studies (for recent examples see Ferguson, 1999; Ellis and Leathers, 1999; Brasnett, 1999). This level of information is also important given that modeled atmospheric response is sensitive to both snow extent and snow depth (Barnett et al. 1989), and coincident SWE and snow covered area anomalies can frequently be of the opposite sign (Derksen et al., 2000a). Additionally, quantitative SWE values for each pixel allows point pattern analysis utilizing such techniques as local indicators of spatial autocorrelation (Derksen et al., 1998a). This level of analysis is impossible with the binary snow/no snow information provided by optical sensors.

Limitations of the passive-microwave approach, however, include large pixel dimensions (making the data suitable for regional, not basin scale applications), and the complicating influence of both snow cover physical properties (see Armstrong et al., 1993; Foster et al., 1999) and overlying vegetation (see Foster et al., 1991; Chang et al., 1997). These factors combine to create temporal and spatial limitations on the appropriate use of passive-microwave retrieved SWE, which will be later discussed in more detail.

The purpose of this study is to apply the growing time series of passive-microwave data to the investigation of associations between terrestrial snow cover and atmospheric circulation. The physical properties of snow cover strongly influence surface reflectance and emission, thereby influencing the energy flux between the surface and atmosphere while synoptic atmospheric circulation drives the deposition and ablation of snow cover. Resolving relationships between snow cover and atmospheric circulation in the context of this dual forcing presents a clear challenge. Various approaches have been adopted which utilize a range of snow cover datasets and atmospheric diagnostics (for a review, see Derksen and LeDrew, in press). Investigation of long time series of data (for example Serreze et al., 1998), model produced fields (for example, Frei and Robinson, 1998), and consideration of forcing conditions such as the El Niño/Southern Oscillation (for example, Cayan, 1996) have all led to an improved understanding of feedbacks between snow

cover and the atmosphere. Further research is required, however, to clarify synoptic scale forcing and time lag relationships.

The specific objectives of this study are

(1) To characterize the variability in North American Prairie SWE distribution through a principal components analysis (PCA) of three similarly derived passive-microwave datasets. The study period for this analysis extends from the winter season (December, January, February) of 1988/89 through 1997/98, at a temporal resolution of five day (pentad) averages. This first analysis phase will address the question

Do consistent SWE patterns reappear from one season to the next?

(2) To investigate the atmospheric patterns (500 mb geopotential height; 700 mb temperature) that correspond to any repeating SWE patterns captured by the PCA. This second analysis phase will address the question

Are unique and consistent atmospheric patterns associated with any repeating modes of SWE?

DATA

Passive-Microwave Derived SWE Imagery

The ability to distinguish snow covered and snow free land in the microwave portion of the electromagnetic spectrum is a function of changes in microwave scatter caused by the presence of snow crystals. For a snow covered surface, microwave brightness temperature decreases with increasing snow depth because the greater number of snow crystals provides increased scattering of the microwave signal. This simple relationship, however, is complicated by a range of physical parameters (Table 1) which place spatial and temporal limitations on the use of passive-microwave imagery for monitoring snow cover.

Table 1. Parameters influencing interaction between microwave energy and snow cover.

Parameter	Influence on Microwave Energy
Snow Wetness	Wet snow approaches black body behaviour; between channel brightness temperature gradient degrades; snow cover becomes “invisible”.
Ice Crusts	Alters absorption and emission characteristics; Increases emissivity at high frequencies relative to low frequencies.
Depth Hoar and Crystal Structure	Large crystals increase snowpack scatter, artificially increasing retrieved SWE.
Snow Depth	At a maximum of approximately 1 metre depth, relationship between brightness temperature and SWE weakens; microwaves are transparent to thin snow (< 3 cm).
Temperature	Large temperature gradients contribute to depth hoar formation; temperature physically associated with snow wetness.
Soil Conditions	Soil type and wetness can influence emissivity.
Vegetative Cover	Wide ranging effects: contributes scatter, absorption, and emission.

The Meteorological Service of Canada (MSC; previously Atmospheric Environment Service) has developed and evaluated single and dual frequency passive-microwave algorithms for determining SWE in the North American Prairies through an intensive satellite/airborne/ground experiment in central Canada (Goodison et al., 1986). An overview of the algorithms, and their strengths and weaknesses, is provided by Goodison and Walker (1994) and is described in the context of time series analysis by Derksen et al. (2000a). The MSC dual frequency algorithm used in this study utilizes the brightness temperature gradient between 19 and 37 GHz Special Sensor Microwave/Imagery (SSM/I) channels in the EASE-Grid (Equal Area SSM/I Earth) projection. Grid spacing is 25 km for the 19 and 37 GHz frequencies, although the actual SSM/I footprint size is 60 and 30 km respectively for these channels. The data were obtained from the National Snow and Ice Data Center in Boulder, Colorado. After processing the brightness temperatures with the dual channel MSC algorithm, a 70 by 40 pixel Prairie subscene was identified for further analysis

(Figure 1). The study area has little physical relief, and is largely agricultural. Winter season land cover is composed of fallow, stubble, pasture, and natural Prairie fields. The passive-microwave scattering environment is therefore relatively simple.

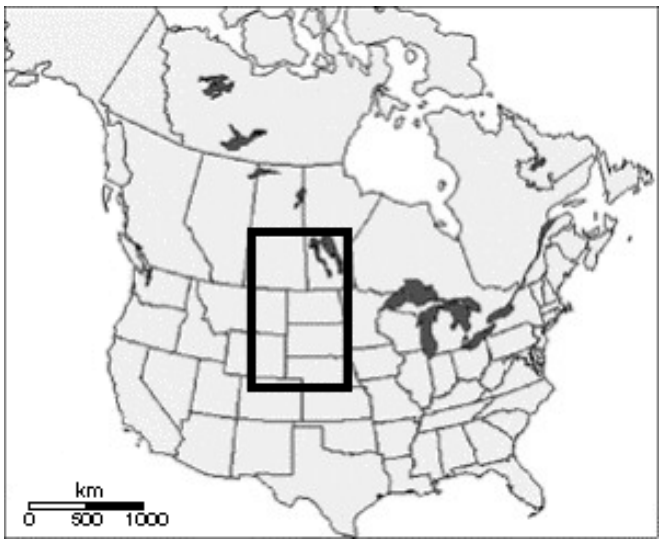

Figure 1. Prairie study area.

The dual frequency algorithm performs strongly when snowpack conditions are deep and dry, achieving 10 to 20 mm agreement with surface sampling (Goodison and Walker, 1994). Problems occur when fresh snow is deposited on a warm surface, and when attempting to discriminate between melting snow areas and snow free land (Walker and Goodison, 1993). For these reasons, winter months were selected for analysis, and data from morning overpass times were used to mitigate the influence of melt. These two decisions have proven to effectively limit regional underestimation of snow cover by the MSC SWE algorithm (Derksen et al., 2000b). The SWE imagery span 10 winter seasons (December, January, February 1988/89 - 1997/98) at a temporal resolution of five days. 18 pentads extend from December 2 to February 29/March 1 as outlined in Table 2. Table 3 summarizes the missing pentads from the time series, which can be attributed to incomplete Prairie coverage within a pentad period primarily caused by data storage and transfer problems on the orbiting platform.

Three ten-season SWE datasets were produced for further analysis:

(1) pentad SWE imagery derived with the MSC dual frequency algorithm
(2) pentad SWE anomaly imagery based on the 10 season mean and standard deviation
(3) pentad change in SWE (hereafter referred to as ΔSWE) imagery calculated by subtracting each SWE pattern from the previous.

Table 2. Summary of pentad structure.

Pentad	**Time Span**	**Pentad**	**Time Span**
68	Dec. 2 to Dec. 6	04	Jan. 16 to Jan. 20
69	Dec. 7 to Dec. 11	05	Jan. 21 to Jan. 25
70	Dec. 12 to Dec. 16	06	Jan. 26 to Jan. 30
71	Dec. 17 to Dec. 21	07	Jan. 31 to Feb. 4
72	Dec. 22 to Dec. 26	08	Feb. 5 to Feb. 9
73	Dec. 27 to Dec. 31	09	Feb. 10 to Feb. 14
01	Jan. 1 to Jan. 5	10	Feb. 15 to Feb. 19
02	Jan. 6 to Jan. 10	11	Feb. 20 to Feb. 24
03	Jan. 11 to Jan. 15	12	Feb. 25 to Feb. 29/March 1

Table 3. Pentads omitted from PCA due to incomplete Prairie coverage.

Season	Omitted Pentads
1988/89	8903
1989/90	None
1990/91	9072
1991/92	9172, 9173
1992/93	9306, 9312
1993/94	9407-9412
1994/95	None

Gridded Atmospheric Data

Atmospheric data were taken from the National Center for Environmental Prediction (NCEP, formerly NMC—National Meteorological Center) gridded data product acquired from NCAR (National Center for Atmospheric Research). This octagonal grid contains 1977 points which appear equally spaced when displayed on a polar stereographic projection. Twice daily atmospheric fields are produced (00 and 12 UTC). Geopotential height, temperature, and wind variables are available for a range of levels, but only two of these variables will be utilized in this study: 500 mb geopotential height (500Z) and 700 mb temperature (700T). A thickness layer field (i.e. 700 mb to 500 mb) would assist in showing system development, but associated research based on Q-vector modelling (LeDrew et al. 1991; LeDrew and Derksen, 1999), which is currently being developed, will provide a stronger indicator.

From the 47 by 51 point NCEP grid an 18 by 18 point region was extracted. This sub-grid covers continental North America, the Arctic Archipelago, and Greenland, and allows examination of synoptic conditions outside the Prairie study area, and their relation to snow cover conditions. Daily data from 00 UTC were averaged for the same pentads as summarized in Table 2 to provide a corresponding time series of atmospheric data.

METHODS

To meet objective one of this study, the three passive-microwave derived SWE datasets were individually subjected to a rotated principal components analysis (PCA) in order to identify the dominant spatial modes within each ten-season time series. PCA mathematically transforms a dataset into a reduced set of uncorrelated variables which represent the majority of the information contained within the original data. The use of principal components simplifies analysis of time series data by representing the entire dataset in a smaller number of images that proportionally explain the variance within the original data. PCA as a time series analysis tool is discussed by Eastman and Fulk (1993) and Piwowar and LeDrew (1996).

For the purposes of this study, three types of output from the PCA are of importance: eigenvalues, eigenvectors, and the component loading pattern. Eigenvalues (λ) define the amount of variance explained by each component, and are commonly expressed as a percentage of the total variance by dividing each individual eigenvalue by the sum of all calculated eigenvalues. Eigenvectors (a) are an intermediate value which define the relationship between the original data and each component. The eigenvectors can be transformed to component loadings by the equation:

$$\text{Loading} = \frac{a \bullet (\lambda)^{1/2}}{\text{variance}^{1/2}}. \quad (1)$$

Because PCA weights the eigenvectors by the square root of the corresponding eigenvalue, the component loadings indicate the correlation between each spatial mode and original pentad spatial pattern on a scale of -1 to +1 (Richman, 1986). A high positive loading means the pentad data are similar to the component, a negative loading indicates an inverse spatial pattern between the

original data and the component. A loading near zero means there is little similarity. A time series plot of the loadings for a given component can therefore be interpreted as an indicator of the temporal persistence of that given spatial mode.

The three SWE time series were orthogonally transformed using the varimax rotation method which maximizes the sum of the variances of the squared loadings within each column of the loadings matrix (Richman, 1986). Each PCA input matrix was composed of columns for each time series pentad, while SSM/I pixels comprised the rows. Not all pentads are represented in the time series because of incomplete study scene coverage (see Table 3), so the input matrix had 168 columns (pentads), and 2800 rows (pixels). PCA was performed using a correlation matrix approach as opposed to a covariance matrix as discussion has shown this method to be advantageous in synoptic climatological applications (Overland and Preisendorfer, 1982). An identical rotated PCA was performed for all three SWE datasets. Comparison of the component loading patterns will allow for an assessment of the three datasets with regards to their suitability for the application of identifying associations with atmospheric circulation.

To meet objective two of this study, composite and anomaly 500Z and 700T fields were computed to temporally correspond to the dominant spatial modes as characterized by the PCA. The anomaly fields were based on the 30-year mean and standard deviation for each pentad, calculated from the years 1961 to 1990. Further discussion and analysis of the composite and anomaly fields will be presented as appropriate.

RESULTS

Do consistent SWE patterns reappear from one season to the next?

The three passive-microwave derived SWE time series were subjected to a rotated principal components analysis (PCA) in order to characterize the dominant spatial modes within each dataset. A summary of the variance explained by the leading components is provided in Table 4. The SWE imagery time series is reduced the most significantly, while the leading ΔSWE components combine to explain less than 50% of the variance.

The motivation behind comparing the three datasets is to identify the most suitable time series for isolating feedbacks with atmospheric circulation. The assumption is that strongly seasonal component loading patterns are not appropriate because the dominant Northern Hemisphere atmospheric circulation patterns tend to reappear within and between seasons. Ideally, the most suitable SWE components will capture spatial modes that also reappear within and between seasons, thereby providing a suitable context for identifying atmospheric patterns that are associated with these repeating snow cover patterns.

First, the component loading pattern for the time series of pentad SWE imagery is shown in Figure 2. The eigenvalue summary in Table 4 shows the SWE time series can be effectively reduced to a relatively small number of components and still characterize the majority of variance in the dataset. The component loading patterns, however, are strongly related to individual winter seasons, illustrating the high degree of interannual variability in Prairie SWE. Only PC1 characterizes a SWE pattern that extends to consecutive, multiple seasons. The remaining components load strongly to individual seasons only, except for PC2, which characterizes both 1993/94 and 1996/97. Because of the seasonal nature of the component loading pattern, the output from the SWE imagery PCA will likely not provide useful information for isolating systematic correlations with winter season North American atmospheric circulation patterns. While one individual component dominates the loading pattern for each season, preliminary analysis has shown that multiple modes of atmospheric circulation occur within individual seasons (Derksen et al., 1998b).

Second, the SWE anomaly loading pattern (Figure 3) illustrates a similar seasonal bias for all leading components. Each component pattern loads strongly (in this case typically in the negative direction due to the positive and negative values in the anomaly images) for single seasons only. Atmospheric patterns do not exhibit temporal persistence of this nature, so like the SWE imagery

discussed previously, this dataset is not well suited for identifying consistent linkages with the atmosphere.

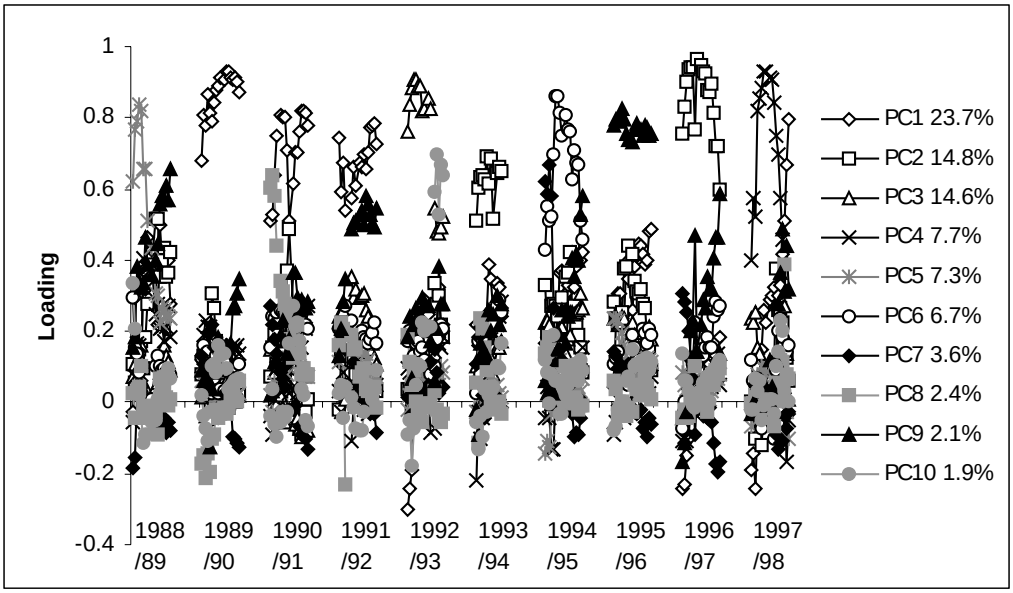

Figure 2. Component loading pattern for the ten-season SWE imagery PCA.

Table 4. Percent variance explained by leading principal components.

Component	SWE Imagery	SWE Anomaly	ΔSWE
PC1	23.7	11.2	16.5
PC2	14.8	10.7	7.5
PC3	14.6	10.3	6.7
PC4	7.7	6.9	5.1
PC5	7.3	5.8	3.9
PC6	6.7	5.1	3.7
PC7	3.6	4.9	2.7
PC8	2.4	4.7	2.7
PC9	2.1	4.3	2.6
PC10	1.9	3.5	2.5
Remainder	15.2	32.6	46.1

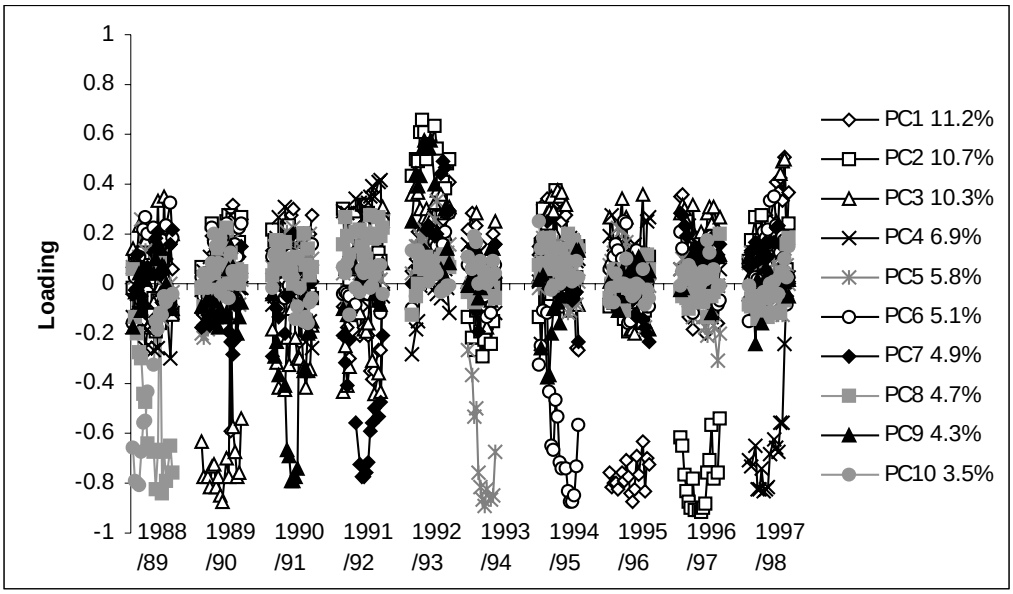

Figure 3. Component loading pattern for the ten-season SWE anomaly PCA.

Finally, the PCA of the ΔSWE time series does produce promising results with respect to the characterization of interseasonally consistent patterns. The loading patterns for the first two ΔSWE components are shown in Figure 4. Both positive and negative phases of these components load strongly for at least one pentad in the majority of seasons through the time series. This allows a positive response to the first research question: are consistent SWE patterns observed to reappear from one season to the next? The answer is yes, but only within the ΔSWE time series. Although the total variance explained by the ΔSWE components is not as high as the other two SWE datasets (Table 4), the nature of the loading pattern means the components produced from this dataset are well suited to investigating associations with atmospheric circulation.

It should be noted that principal components do not depict actual observable data patterns, but rather variance presumed to be evident in all cases. The spatial patterns of the most highly loaded pentads are, therefore, ideally suited for the interpretation of physical processes to ensure the identification of real spatial patterns. In this study, those pentads of ΔSWE imagery which loaded strongly (negatively or positively) to PC1 or PC2 were averaged to produce composite component images. In Figure 4, solid black diamonds represent the ΔSWE images used to produce the composite patterns that depict the positive and negative phases of components 1 and 2. These composite images are shown in Figure 5. Positive ΔSWE values indicate regions of snow accumulation from the previous SWE pattern, while negative values correspond to regions of snow ablation.

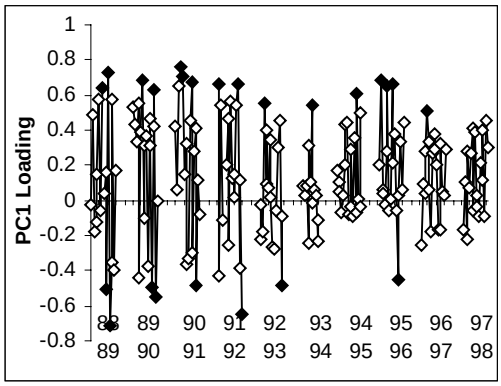

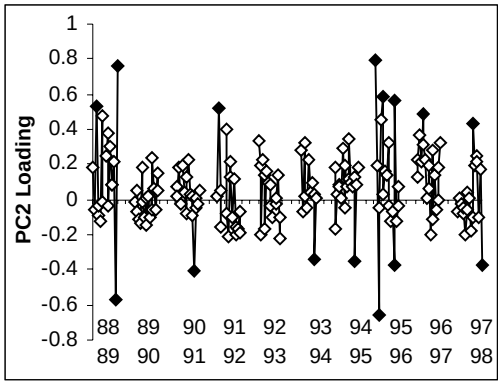

Figure 4. Component loading pattern for the ten-season ΔSWE PC1 (top) and PC2 (bottom). Solid black diamonds represent those ΔSWE images used to produce the composite patterns to illustrate the positive and negative phases of each component.

The positive phase of PC1 captures a pattern of a widespread increase in SWE values across the northern portion of the study area, with a decrease in SWE values observed across the south. The negative phase of PC1 depicts a reversal of these broad accumulation and ablation zones. PC2 is characterized by a meridional zone of activity in SWE which bisects the study area, oriented from the northwest to the southeast. In the positive phase, this is a meridional accumulation zone, while in the negative phase it reverses to become a zone of ablation.

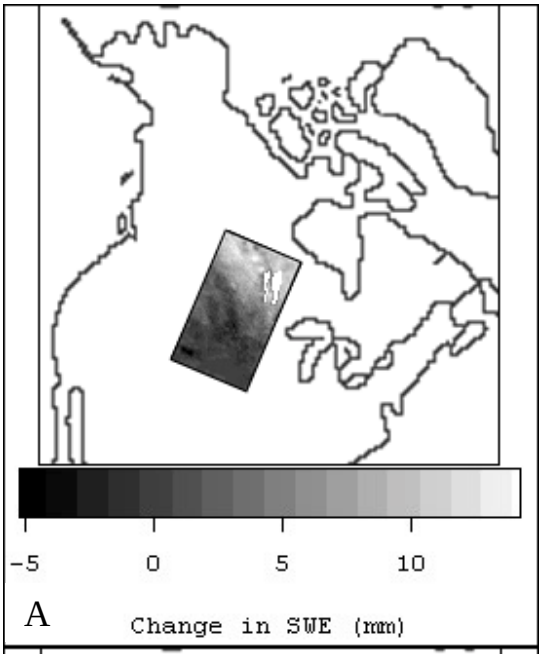

A

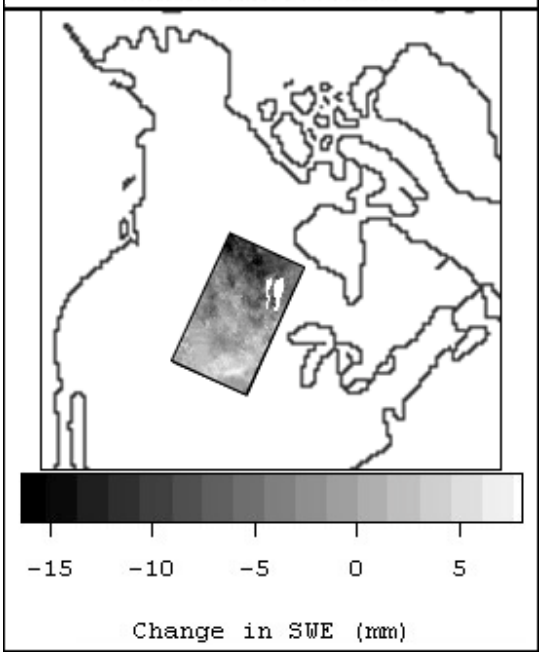

B

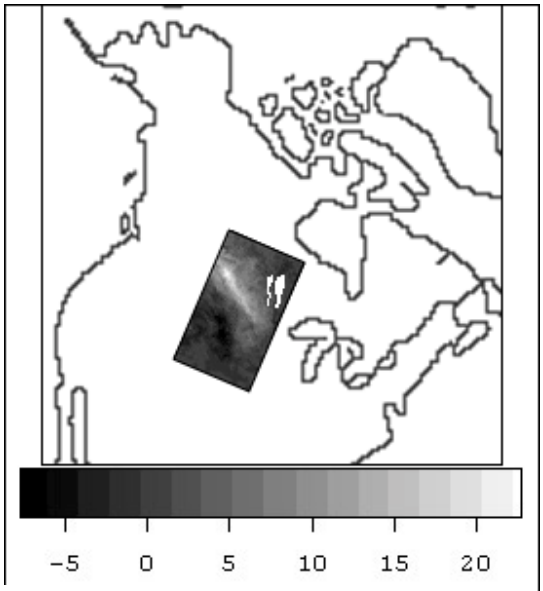

C

D

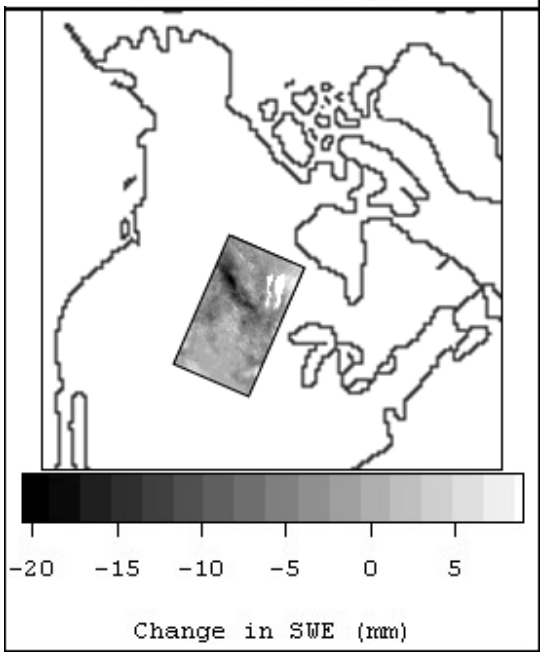

Figure 5. Composite images which characterize the positive (A) and negative (B) phases of ΔSWE PC1, and the positive (C) and negative (D) phases of ΔSWE PC2.

In summary, the ΔSWE time series produces PCA results appropriate for investigating links with the atmosphere, when compared to SWE imagery and SWE anomaly datasets. The component loading patterns in Figure 4 illustrate that the four ΔSWE patterns shown in Figure 5 reappear throughout the ten season time series. It is now possible to proceed to objective two of this study, and investigate whether consistency exists in the atmospheric patterns associated with these repeating modes of SWE.

Are unique and consistent atmospheric patterns associated with any repeating modes of SWE?

In order to investigate the atmospheric patterns associated with the positive and negative phases of the first two ΔSWE components, 500Z and 700T composite and anomaly fields were derived. Atmospheric data were taken from the NCEP gridded data product. As shown in Figure 4, pentads which load most strongly to the positive and negative phases of ΔSWE PC1 and PC2 were used to derive the component patterns shown in Figure 5. Those strongly loading pentads from 1988/89 through 1997/99 (as marked in Figure 4) were used to calculate the atmospheric composites and anomalies that correspond at no time lag to the component patterns. Only the anomalies will be illustrated due to space limitations.

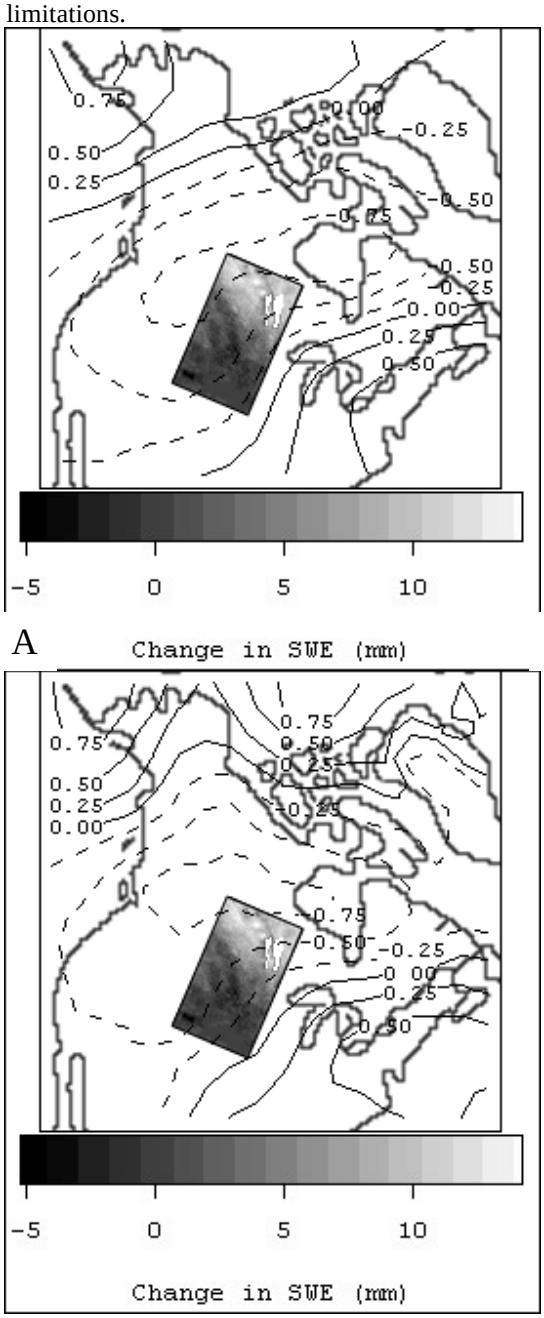

Figure 6. 500Z anomaly (A), and 700T anomaly (B) fields, which correspond to the positive phase of ΔSWE PC1.

The 500Z and 700T anomaly fields for those pentads that load most strongly to the positive and negative phases of PC1 and PC2 are shown in Figures 6 through 9. As described earlier, the positive phase of ΔSWE PC1 characterizes snow ablation in the south, and accumulation in the north of the study area. Associated with this SWE pattern is a trough pattern of geopotential height across the Prairies with anomalous low pressure oriented in a cell from west to east (Figure 6a). The temperature anomaly field shows a similar pattern (Figure 6b), with below normal temperatures over the majority of the study area.

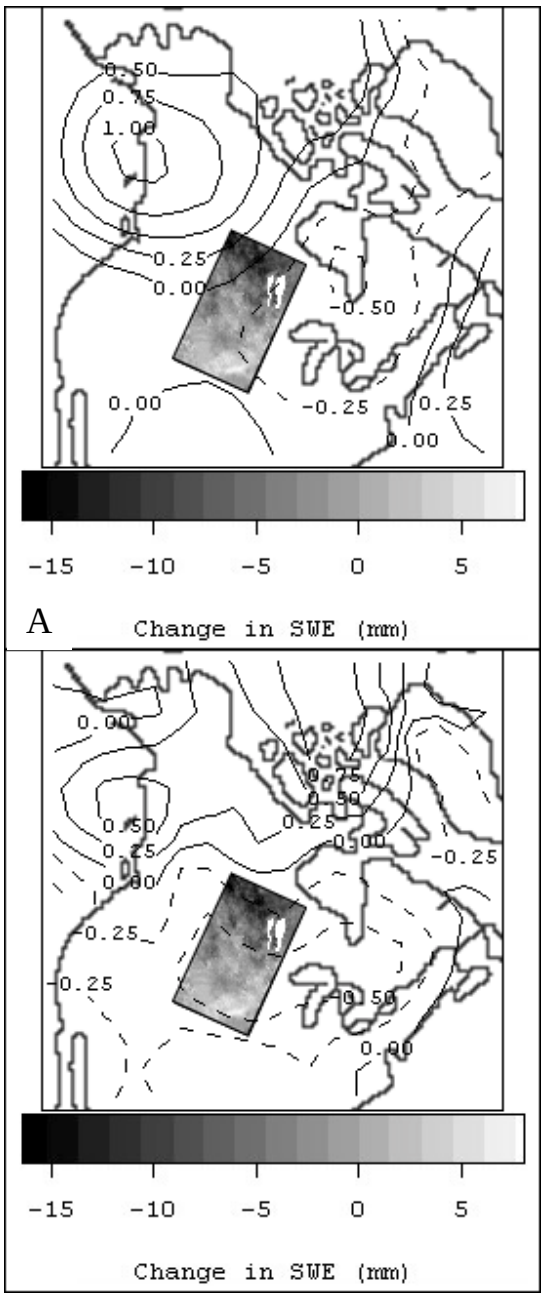

Figure 7. 500Z anomaly (A), and 700T anomaly (B) fields, which correspond to the negative phase of ΔSWE PC1.

The negative phase of ΔSWE PC1 depicts a reversal of the positive phase with snow ablation in the north, and accumulation in the south. The composite 500Z pattern indicates a shift from the trough pattern associated with the positive component, to a Prairie ridge formed by anomalously high geopotential height centered over the northern Pacific coast (Figure 7a). The temperature anomaly pattern (Figure 7b) is similar to that related to the positive phase of this SWE component—negative temperatures are present over the study area. The cold cell, however, is shifted southwards, with the strongest temperature departures now centered over the southern Prairies as opposed to the northern Prairies.

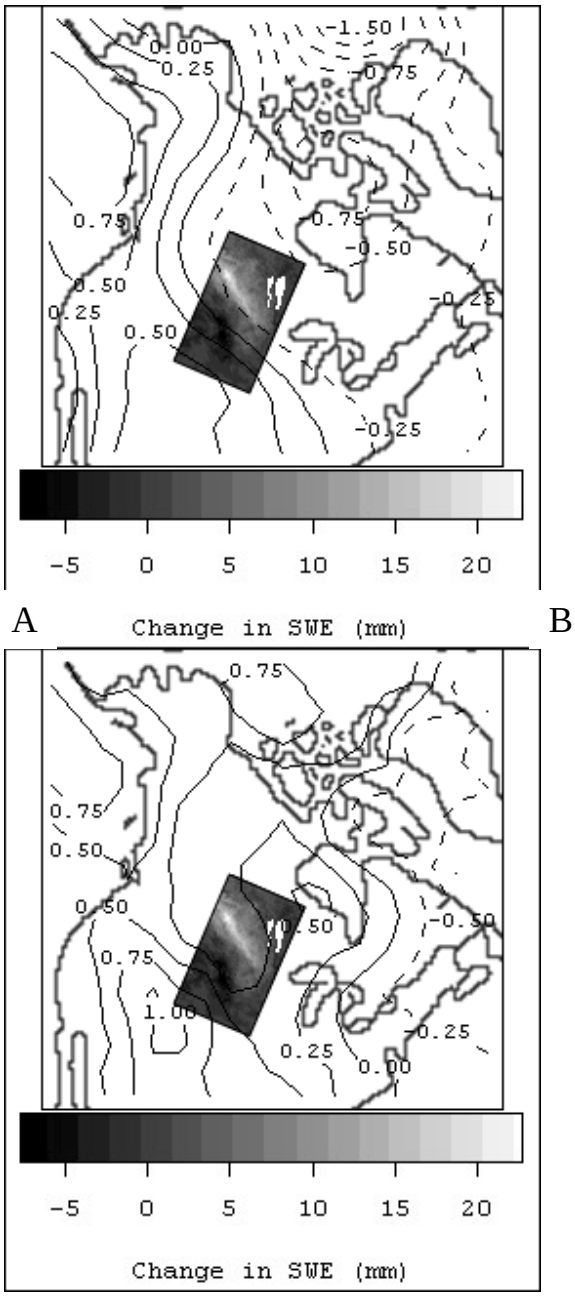

Figure 8. 500Z anomaly (A), and 700T anomaly (B) fields, which correspond to the positive phase of ΔSWE PC2.

The positive phase of ΔSWE PC2 highlights an accumulation zone extending from the northwest of the study area to the southeast. Atmospheric airflow is oriented in the same meridional direction with negative geopotential height anomalies forming a clear boundary at the southern margin of the accumulation zone (Figure 8a). The temperature anomalies are less coherently associated with the accumulation area (Figure 8b).

Atmospheric airflow is again aligned with the active SWE zone in the negative phase of ΔSWE PC2. While a trough and negative height anomalies were associated with PC2 positive, Prairie ridging and positive height anomalies (Figure 9a) are linked to PC2 negative. Perhaps as a consequence, SWE ablation is observed rather than SWE accumulation. A cell of anomalously warm temperatures is centered over the study area (Figure 9b).

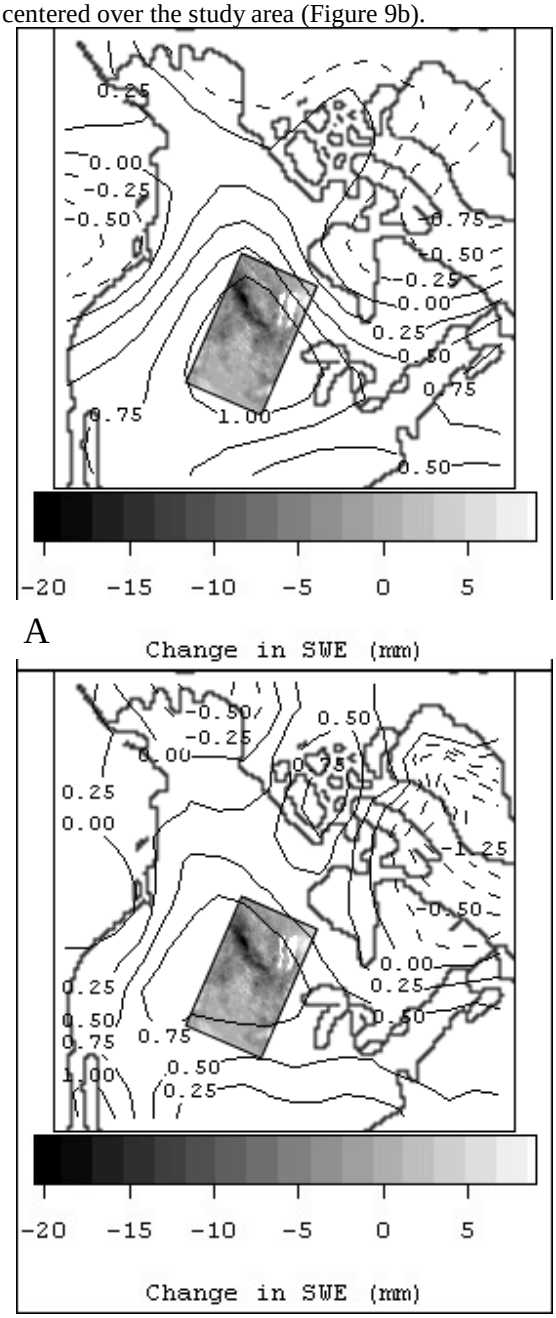

Figure 9. 500Z anomaly (A), and 700T anomaly (B) fields, which correspond to the negative phase of ΔSWE PC2.

The patterns shown in Figures 6 through 9 present the mean atmospheric anomalies associated with the repeating modes of Prairie snow cover as captured by the rotated PCA. These results show that unique atmospheric circulation patterns are associated with each phase of the first two ΔSWE components. These fields, however, are mathematical constructs only. In order to identify the consistency of the atmospheric patterns associated with each of the ΔSWE components, the atmospheric fields that correspond temporally to each phase of the components (as noted in Figure 4) were subjected to a rotated PCA to assess the within-group variability. The greater the similarity within each group, the greater the variance that will be explained by the leading component. The greater the similarity within groups, the greater the predictive potential of this analysis.

The results of the within-group PCA are shown in Table 5. They are encouraging with respect to the identification of consistent atmospheric patterns associated with each phase of the first two ΔSWE components. The first component explains over 80% of the variance within each group, while the average loading is near or over 0.9 in all cases. These results indicate that the atmospheric patterns (both 500Z and 700T) which occur simultaneously to the ΔSWE patterns characterized by PC1 and PC2 are spatially consistent. Therefore, the atmospheric composites and anomalies shown in Figures 6 through 9 are relevant patterns that can be linked to the specific SWE accumulation and ablation events captured by the ΔSWE components.

Table 5. Summary of 500Z and 700T within-group PCA results. Input pentads to the are noted in Figure 4.

	500Z		700T	
	% Variance Explained, PC1	Average Loading, PC1	% Variance Explained, PC1	Average Loading, PC1
SWE PC1 +	85.0	0.920	87.8	0.936
SWE PC1 -	82.4	0.906	81.1	0.899
SWE PC2 +	89.7	0.947	86.9	0.932
SWE PC2 -	89.8	0.947	88.9	0.943

DISCUSSION AND CONCLUSIONS

The growing time series of passive-microwave imagery can provide an ideal dataset for examining variability in terrestrial snow cover, although spatial and temporal algorithm limitations can place constraints on this data source. The goal of this study was to apply passive-microwave data to the investigation of associations between winter season North American Prairie SWE patterns and atmospheric circulation. Two main research questions were investigated:

(1) Do consistent SWE patterns reappear from one season to the next?

(2) Are unique and consistent atmospheric patterns associated with any repeating modes of SWE?

A rotated PCA was used to compare three passive-microwave derived SWE datasets: SWE imagery, SWE anomalies, and ΔSWE. The results indicate that the ΔSWE time series is the most suitable for identifying associations with atmospheric circulation because unlike the first two time series, the leading components isolate SWE patterns which repeat within and between seasons. Given that preferred spatial modes of Northern Hemisphere atmospheric circulation also exhibit this temporal behaviour, the first two ΔSWE components were used for further analysis.

These two retained components characterize, in their positive and negative phases, four dominant modes of ΔSWE which are evident throughout the ten season time series. The positive (negative) phase of principal component 1 captures a pattern of widespread SWE ablation (accumulation) in the south with accumulation (ablation) to the north. The positive (negative) phase of principal component two characterizes a meridional accumulation (ablation) zone oriented from the northwest to southeast of the study area.

500 mb geopotential height and 700 mb temperature composite and anomaly fields were produced from the pentads which coincide with the strongest ΔSWE component loadings. A comparison of these composite and anomaly fields shows that unique mean atmospheric conditions are associated with each phase of the components. Rotated PCA of the atmospheric patterns associated with each component phase showed that a single component explained the vast majority of within-group variance. This finding affirms that spatially consistent and unique atmospheric patterns are associated each phase of the two leading ΔSWE components. A summary description of the atmospheric composite and anomaly patterns is provided in Table 6.

Table 6. Summary of composite and anomaly fields associated with change in SWE components.

	500Z		700T	
ΔSWE Pattern	Composite	Anomaly	Composite	Anomaly
Accumulation in north, ablation in south	Prairie trough	Negative height departures across prairies	Trough pattern	Cold departures centered over northern prairies
Ablation in north, accumulation in south	Ridge to west of prairies	No height departures	Ridge pattern	Cold departures centered over southern prairies
Meridional zone of accumulation	Meridional flow	Negative height departures over accumulation zone	Meridional pattern	Warm departures over prairies
Meridional zone of ablation	Prairie ridge	Positive height departures across prairies	Meridional pattern	Warm departures over prairies

Cold temperature departures are associated with both phases of ΔSWE PC1. With the positive phase of PC1 (snow accumulation in the north), the cold cell is located over the northern portion of the study area, while it shifts to the south with the negative phase of PC1 (snow accumulation in the south). While this shift in cold cell location is very subtle, the spatial pattern of SWE accumulation and ablation reverses completely. Warm temperature departures, conversely, are associated with both phases of ΔSWE PC2, although again, the warm cell location differs between the two component phases. Since like-direction temperature departures are linked to both the positive and negative phases of each ΔSWE component, it appears that atmospheric temperature alone is a poor explanatory variable.

Variability in the location of a western North American ridge and eastern Arctic low account for the differences in the 500Z composites. These results are consistent with the findings of Frei and Robinson (1999). They found that western North American snow cover is controlled by the longitudinal location of the North American ridge, while eastern North American snow cover is associated with a dipole 500Z pattern with centers over southern Greenland and the midlatitude North Atlantic.

The 500Z anomaly fields associated with the negative phases of ΔSWE PC1 and PC2 depict positive height departures over western North America and negative height departures over eastern North America. This pattern is similar in structure to the Pacific North America (PNA) teleconnection index, which has been linked in low-frequency studies to deficit snow cover in western North America (for example, Gutzler and Rosen, 1992). The results of this study indicate that 'PNA type' patterns may be linked to regions of Prairie snow ablation at the synoptic scale.

This analysis has shown that unique atmospheric circulation patterns can be associated with consistent patterns of ΔSWE which appear within and between seasons. The method was to isolate repeating SWE patterns first, and then investigate the temporally coincident atmospheric circulation patterns second. This approach may be necessary because recent analysis shows that 500 mb circulation patterns that can be linked to snow cover are often of a secondary nature, and are therefore not captured as leading components of geopotential height fields (Frei and Robinson

1999). Systematic correlations of SWE and atmospheric components may, therefore, not contribute meaningful results.

Remaining to be addressed are the potential presence of time lags in the feedback relationships presented here. Investigating atmospheric data that both leads and lags the ΔSWE components used in this analysis will assist in this direction, but is beyond the scope of this study. Additionally, integrating atmospheric teleconnections as they relate to repeating SWE patterns may also prove insightful. With a growing time series of synoptically sensitive, quantitative SWE imagery, the passive-microwave time series should prove helpful in resolving forcing relationships between terrestrial snow cover and atmospheric circulation.

ACKNOWLEDGMENTS

This work was supported by funding through the Meteorological Service of Canada Science Subvention and CRYSYS contract to E. LeDrew, and the Natural Science and Engineering Research Council (Operating Grant - E. LeDrew; Scholarship - C. Derksen). Thanks are extended to Joseph Piwowar for assistance with data processing. The SSM/I EASE-Grid data were obtained from the EOSDIS National Snow and Ice Data Center Distributed Active Archive Center (NSIDC DAAC), University of Colorado at Boulder.

REFERENCES

Armstrong, R., A. Chang, A. Rango and E. Josberger. 1993. Snow depths and grain-size relationships with relevance for passive-microwave studies. Annals of Glaciology. 17: 171-176.

Barnett, T., L Dumenil, U. Schlese, E. Roeckner, and M. Latif. 1989. The effect of Eurasian snow cover on regional and global climate variations. Journal of the Atmospheric Sciences. 46(5): 661-685.

Brasnett, B. 1999. A global analysis of snow depth for numerical weather prediction. Journal of Applied Meteorology. 38: 726-740.

Cayan, D. 1996. Interannual climate variability and snowpack in the Western United States. Journal of Climate. 9(5): 928-948.

Chang, A., J. Foster, D. Hall, B. Goodison, A. Walker, J. Metcalfe, and A. Harby. 1997. Snow parameters derived from microwave measurements during the BOREAS winter field campaign. Journal of Geophysical Research. 102(D24): 29 663-29 671.

Chang, A., J. Foster, and D. Hall. 1990. Satellite sensor estimates of northern hemisphere snow volume. International Journal of Remote Sensing. 11(1): 167-171.

Derksen, C., M. Wulder, E. LeDrew, and B. Goodison. 1998a. Associations between spatially autocorrelated patterns of SSM/I derived Prairie snow cover and atmospheric circulation. Hydrological Processes. 12(15): 2307-2316.

Derksen, C., E. LeDrew, and B. Goodison. 1998b. SSM/I derived snow water equivalent data: the potential for investigating linkages between snow cover and atmospheric circulation. Atmosphere-Ocean. 36(2): 95-117.

Derksen, C., E. LeDrew, and B. Goodison. 2000a. Temporal and spatial variability of North American Prairie snow cover (1988 to 1995) inferred from passive-microwave derived snow water equivalent (SWE) imagery. Water Resources Research. 36(1): 255-266.

Derksen, C., E. LeDrew, A. Walker, and B. Goodison. 2000b. The influence of sensor overpass time on passive-microwave retrieval of snow cover parameters. Remote Sensing of Environment. 71(3): 297-308.

Derksen C., and E. LeDrew. In press. Variability and change in terrestrial snow cover: data acquisition and links to the atmosphere. Progress in Physical Geography.

Eastman, J., and M. Fulk. 1993. Long sequence time series evaluation using standardized principal components. Photogrammetric Engineering and Remote Sensing. 59(8): 1307-1312.

Ellis, A., and D. Leathers. 1999. Analysis of cold airmass temperature modification across the U.S. Great Plains as a consequence of snow depth and albedo. Journal of Applied Meteorology. 38: 696-711.
Ferguson, R. 1999. Snowmelt runoff models. Progress in Physical Geography. 23(2): 205-227.
Foster, J., A. Chang, D. Hall, and A. Rango. 1991. Derivation of snow water equivalent in boreal forests using microwave radiometry. Arctic. 44(Supp. 1): 147-152.
Foster, J., D. Hall, A. Chang, A. Rango, W. Wergin, and E. Erbe. 1999. Effects of snow crystal shape on the scattering of passive-microwave radiation. IEEE Transactions on Geoscience and Remote Sensing. 37(2): 1165-1168.
Frei, A., and D. Robinson. 1998. Evaluation of snow extent and its variability in the Atmospheric Model Intercomparison Project. Journal of Geophysical Research. 103(D8): 8859-8872.
Frei, A., and D. Robinson. 1999. Northern Hemisphere snow extent: regional variability 1972-1994. International Journal of Climatology. 19: 1535-1560.
Goodison, B., I. Rubinstein, F. Thirkettle, and E. Langham. 1986. Determination of snow water equivalent on the Canadian Prairies using microwave radiometry. Modelling Snowmelt Induced Processes, Proceedings of the Budapest Symposium, July 1986. 163-173.
Goodison, B., and A. Walker. 1994. Canadian development and use of snow cover information from passive-microwave satellite data. In Choudhury, B., Y. Kerr, E.Njoku, and P. Pampaloni (eds.). Passive-microwave Remote Sensing of Land-Atmosphere Interactions. VSP BV, Utrecht, Netherlands, 245-262.
Grody, N., and A. Basist. 1996. Global identification of snowcover using SSM/I measurements. IEEE Transactions on Geosciences and Remote Sensing. 34(1):237-249.
Gutzler, D., and R. Rosen. 1992. Interannual variability of wintertime snow cover across the Northern Hemisphere. Journal of Climate 5:1441-1447.
LeDrew, E., D. Johnson, and J. Maslanik. 1991. An examination of the atmospheric mechanisms that may be responsible for the annual reversal of the Beaufort sea ice field. International Journal of Climatology. 11: 841-859.
LeDrew, E., and C. Derksen. 1999. SSM/I imagery of sea ice, Q-vectors and synoptic-scale linkages between the atmosphere and cryosphere: eighteen years of variability in the Beaufort Sea. The example of principal component one of sea ice. CD-ROM Proceedings, International Geoscience and Remote Sensing Symposium, Hamburg, Germany, July, 1999.
Overland, J., and R. Preisendorfer. 1982. A significance test for principal components applied to a cyclone climatology. Monthly Weather Review. 110(1): 1-4.
Piwowar, J., and E. LeDrew. 1996. Principal components analysis of Arctic ice conditions between 1978 and 1987 as observed from the SMMR data record. Canadian Journal of Remote Sensing. 22(4): 390-403.
Richman, M. 1986. Rotation of principal components. Journal of Climatology. 6: 293-335.
Serreze, M., M. Clark, D. McGinnis, and D. Robinson. 1998. Characteristics of snowfall over the eastern half of the United States and relationships with principal modes of low-frequency atmospheric variability. Journal of Climate. 11: 234-250.
Tait, A. 1998. Estimation of snow water equivalent using passive-microwave radiation data. Remote Sensing of Environment. 64: 286-291.
Walker, A. and B. Goodison. 1993. Discrimination of a wet snow cover using passive-microwave satellite data. Annals of Glaciology. 17: 307-311.